The Discrete Cones Method for Two-Dimensional Neutron Transport Computation in General Media

Yoichi Watanabe and Charles W. Maynard

October 1984

UWFDM-599

FUSION TECHNOLOGY INSTITUTE

UNIVERSITY OF WISCONSIN

MADISON WISCONSIN

The Discrete Cones Method for Two-Dimensional Neutron Transport Computation in General Media

Yoichi Watanabe and Charles W. Maynard

Fusion Technology Institute
University of Wisconsin
1500 Engineering Drive
Madison, WI 53706

http://fti.neep.wisc.edu

October 1984

UWFDM-599

THE DISCRETE CONES METHOD FOR TWO-DIMENSIONAL NEUTRON TRANSPORT COMPUTATION IN GENERAL MEDIA

Yoichi Watanabe and Charles W. Maynard

Fusion Technology Institute
Nuclear Engineering Department
University of Wisconsin-Madison
Madison, Wisconsin 53706

October 1984

UWFDM-599

TABLE OF CONTENTS

1. INTRODUCTION

We have been developing the discrete cones method (the DC_N method) for two-dimensional neutron transport computation. The general theory of the DC_N method was already reported.[1] A hybrid method was created by applying the DC_N method to a solution in a void and the S_N method to a solution in non-void regions. The method was formulated for both X-Y[1] and R-Z geometry.[2] The numerical experiments demonstrate the strong mitigation of the ray effects in a void.

In the present paper we formulate the DC_N method for a solution in a non-void region. Our goal is to obtain a two-dimensional neutron transport computational method which is free of the ray effects and at the same time as efficient as the S_N method. In Sections 2 and 3, the DC_N method will be constructed for X-Y geometry. Section 4 will describe new programs utilizing the DC_N method. In Section 5 several sample problems will be solved to show the capability and numerical properties of the method. Section 6 will conclude the report.

2. CONSTRUCTION OF THE DISCRETE CONES METHOD

In this chapter, we shall discuss an application of the discrete cones method to solutions of the neutron transport equation in a non-void. As we mentioned, we expect ray effect mitigation by this method. However, the application is restricted to solutions in X-Y geometry.

The spatial domain of a system is partitioned into rectangular mesh cells, D_i. In a cell D_i, we solve the integral form of the transport equation:

$$\Psi(\underline{r},\underline{\Omega}) = \int_0^{s_0} ds\, S(\underline{r}',\underline{\Omega}) e^{-\alpha(\underline{r}',\underline{r})} + \Psi(\underline{r}_s,\underline{\Omega}) e^{-\alpha(\underline{r}_s,\underline{r})} \qquad (1)$$

where $\underline{r}_s$ is a point where a particle enters the mesh cell, $\underline{r}$ is a point where the particle leaves the mesh cell, $s = |\underline{r}' - \underline{r}|$, $s_o = |\underline{r}_s - \underline{r}|$, and $\alpha(\underline{r}',\underline{r})$ is the optical length defined by $\alpha(\underline{r}',\underline{r}) = \int_0^s \sigma_t(\underline{r} - s\underline{\Omega})\, ds$.

First, we assume uniform composition of a material over the mesh cell D_i. This leads to $\alpha(\underline{r}',\underline{r}) = \sigma_{ti}s$ and $\alpha(\underline{r}_s,\underline{r}) = \sigma_{ti}s_o$, where σ_{ti} denotes the total macroscopic cross section of the cell D_i. Second, we assume that the source term $S(\underline{r}',\underline{\Omega})$, which includes the scattering, fission, and external source terms, is constant over the mesh cell D_i. This leads to $S(\underline{r}',\underline{\Omega}) = S_i(\underline{\Omega})$. Under the above assumptions, performing the integration with respect to s in Eq. (1) results in

$$\Psi(\underline{r},\underline{\Omega}) = \frac{1}{\sigma_{ti}}\left(1 - e^{-\sigma_{ti}s_o}\right)S_i(\underline{\Omega}) + \Psi(\underline{r}_s,\underline{\Omega})e^{-\sigma_{ti}s_o}. \tag{2}$$

To find the transfer and escape matrix elements, we consider a rectangular mesh cell in an X-Y coordinate system as illustrated in Fig. 1. Multiplying Eq. (2) by $\underline{\Omega}\cdot\underline{n}_T$ and integrating it over the surface TOP and the m'th cone, $\Delta\Omega_m = [\xi_{m-1/2},\xi_{m+1/2}]\times[\psi_{m-1/2},\psi_{m+1/2}]$, we have

$$\begin{aligned}
&\int_{x_L}^{x_R} dx \iint_{\Delta\Omega_m} d\xi\, d\psi\, (\underline{\Omega}\cdot\underline{n}_T)\, \Psi(x,y_T,\xi,\psi) \qquad (3)\\
&\quad = \frac{1}{\sigma}\int_{x_L}^{x_R} dx \iint_{\Delta\Omega_m} d\xi d\psi\, (\underline{\Omega}\cdot\underline{n}_T)\left(1 - e^{-\sigma s_o}\right) S(\xi,\psi)\\
&\qquad + \int_{x_L}^{x_R} dx \iint_{\Delta\Omega_m} d\xi d\psi\, (\underline{\Omega}\cdot\underline{n}_T)\, \Psi(\underline{r}_s,\xi,\psi)e^{-\sigma s_o},
\end{aligned}$$

where we omit the subscript i and abbreviate σ_t to σ. It is noted that s_o depends on the outgoing point of a particle on the surface TOP and its di-

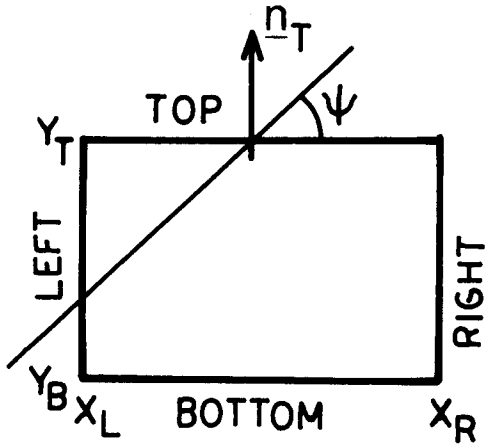

Fig. 1 Schematic diagram of a mesh cell.

rection. Using $\underline{\Omega}\cdot\underline{n}_T = \sqrt{1-\xi^2}\sin\psi$, and assuming the angular flux Ψ is constant over the m'th cone, we can integrate the left-hand side of Eq. (3) to find

$$\text{L.H.S.} = g_m \, \Delta x \, \Delta\mu_m \, \Psi_{Tm} \tag{4}$$

where: $$g_m = \int_{\xi_-}^{\xi_+} \sqrt{1-\xi^2}\, d\xi = \frac{1}{2}\left[\xi\sqrt{1-\xi^2} + \arcsin\,\xi\right]_{\xi_-}^{\xi_+} ,$$

$$\Delta\mu_m = \int_{\psi_-}^{\psi_+} \sin\psi\, d\psi = \cos\psi_- - \cos\psi_+ ,$$

$$\Delta x = x_R - x_L ,$$

and Ψ_{Tm} is the m'th cone flux on the surface TOP. From now on, $\xi_{m\pm1/2}$ and $\psi_{m\pm1/2}$ are abbreviated to $\xi_\pm$ and $\psi_\pm$, respectively. The right-hand side of Eq. (3) is rearranged as follows:

$$\text{R.H.S.} = \int_{x_L}^{x_R} dx \iint_{\Delta\Omega_m} d\xi d\psi \sqrt{1-\xi^2}\sin\psi \frac{S(\xi,\psi)}{\sigma} \tag{5}$$

$$+ \int_{x_L}^{x_R} dx \iint_{\Delta\Omega_m} d\xi d\psi \sqrt{1-\xi^2}\sin\psi e^{-\sigma s_0}\left[\Psi(\underline{r}_s,\xi,\psi) - S(\xi,\psi)/\sigma\right] .$$

To go further, we point out an advantage for using X-Y geometry. In X-Y geometry, if a particle lies in a cone at a point, the particle lies in the cone forever as long as it streams without collisions. In contrast, in curved geometries a particle moves over several cones as it streams. This makes the discrete cones method in curved geometries much more difficult than in X-Y geometry.

Now, taking account of the above fact for X-Y geometry, we perform the integrations in Eq. (5). First, we define τ by $\tau = \cos \psi$. From the geometry shown in Fig. 1, we see that

$$s_o = (x - x_L)/\mu$$

for particles streaming from LEFT to TOP, and

$$s_o = \Delta y/\eta$$

for particles streaming from BOTTOM to TOP, where $\Delta y = y_T - y_B$, $\mu = \sqrt{1 - \xi^2}\ \tau$, and $\eta = \sqrt{1 - \xi^2}\ \sqrt{1 - \tau^2}$. Furthermore, we define ψ_o, τ_o, and $\tau_\pm$ by

$$\psi_o = \arctan\left(\frac{\Delta y}{\Delta x}\right),$$

$$\tau_o = \cos \psi_o ,$$

and

$$\tau_\pm = \cos \psi_\mp .$$

Now we treat the second term of Eq. (5) separately. By assuming that $\Psi(\underline{r}_s, \xi, \psi) - S(\xi, \psi)/\sigma$ is constant over the m'th cone, this is replaced by $\Psi_{-m} - S_m/\sigma$, where Ψ_{-m} is either Ψ_{Bm} or Ψ_{Lm}. When $\tau_o < \tau_-$, all the particles crossing TOP in the m'th cone come from LEFT. Hence, the second term of Eq. (5), I_2, becomes

$$I_2 = \{\int_{x_L}^{x_R} dx \int_{\xi_-}^{\xi_+} \int_{\tau_-}^{\tau_+} \sqrt{1-\xi^2}\, d\xi d\tau \exp\left(-\frac{\sigma(x - x_L)}{\sqrt{1-\xi^2}\,\tau}\right)\}\left(\Psi_{Lm} - \frac{S_m}{\sigma}\right) .$$

To simplify the integration with respect to the variable ξ, we include $\sqrt{1-\xi^2}$ in the g_m and set ξ to ξ_m. As a result, I_2 becomes

$$I_2 = g_m C_{31}(\Psi_{Lm} - S_m/\sigma) , \tag{6}$$

where

$$C_{31} = \int_{x_L}^{x_R} dx \int_{\tau_-}^{\tau_+} d\tau \exp\left(-\frac{\sigma_p(x - x_L)}{\tau}\right) \tag{7}$$

and

$$\sigma_p = \frac{\sigma}{\sqrt{1-\xi_m^2}} .$$

Next, we define x_1, x_2, and $\hat{\tau}(x)$ by

$$\tau_- = \frac{x_1 - x_L}{\sqrt{(x_1 - x_L)^2 + \Delta y^2}} ,$$

$$\tau_+ = \frac{x_2 - x_L}{\sqrt{(x_2 - x_L)^2 + \Delta y^2}} ,$$

and

$$\hat{\tau}(x) = \frac{x - x_L}{\sqrt{(x - x_L)^2 + \Delta y^2}} .$$

When $\tau_- \leq \tau_0 \leq \tau_+$, we see that some of the particles crossing TOP in the m'th cone come from LEFT if $\tau_- \leq \tau \leq \tau_+$, and $x_L \leq x \leq x_1$, or $\hat{\tau} \leq \tau \leq \tau_+$ and $x_1 \leq x \leq x_R$. Others come from BOTTOM if $\tau_- \leq \tau \leq \hat{\tau}$ and $x_1 \leq x \leq x_R$. Thus, I_2 is expressed by

$$I_2 = \int_{x_L}^{x_1} dx \int_{\xi_-}^{\xi_+} \int_{\tau_-}^{\tau_+} \sqrt{1-\xi^2}\, d\xi d\tau \exp\left(-\frac{\sigma(x-x_L)}{\sqrt{1-\xi^2}\,\tau}\right)\left(\Psi_{Lm} - \frac{S_m}{\sigma}\right)$$

$$+ \int_{x_1}^{x_R} dx \int_{\xi_-}^{\xi_+} \int_{\hat{\tau}(x)}^{\tau_+} \sqrt{1-\xi^2}\, d\xi d\tau \exp\left(-\frac{\sigma(x-x_L)}{\sqrt{1-\xi^2}\,\tau}\right)\left(\Psi_{Lm} - \frac{S_m}{\sigma}\right)$$

$$+ \int_{x_1}^{x_R} dx \int_{\xi_-}^{\xi_+} \int_{\tau_-}^{\hat{\tau}(x)} \sqrt{1-\xi^2}\, d\xi d\tau \exp\left(-\frac{\sigma\Delta y}{\sqrt{1-\xi^2}\,\sqrt{1-\tau^2}}\right)\left(\Psi_{Bm} - \frac{S_m}{\sigma}\right).$$

By the assumption made for the ξ variable, I_2 becomes

$$I_2 = g_m\left\{C_{32}\left(\Psi_{Lm} - \frac{S_m}{\sigma}\right) + C_{33}\left(\Psi_{Bm} - \frac{S_m}{\sigma}\right)\right\}, \tag{8}$$

where

$$C_{32} = \int_{x_L}^{x_1} dx \int_{\tau_-}^{\tau_+} d\tau \exp\left(-\frac{\sigma_p(x-x_L)}{\tau}\right) + \int_{x_1}^{x_R} dx \int_{\hat{\tau}(x)}^{\tau_+} d\tau \exp\left(-\frac{\sigma_p(x-x_L)}{\tau}\right), \tag{9}$$

and

$$C_{33} = \int_{x_1}^{x_R} dx \int_{\tau_-}^{\tau_+} d\tau \exp\left(-\frac{\sigma_p \Delta y}{\sqrt{1-\tau^2}}\right). \tag{10}$$

When $\tau_+ < \tau_0$, the particles come from LEFT either for $\tau_- < \tau < \tau_+$ and $x_L < x < x_1$, or $\hat{\tau}(x) < \tau < \tau_+$ and $x_1 < x < x_2$; meanwhile, they come from BOTTOM either for $\tau_- < \tau < \hat{\tau}(x)$ and $x_1 < x < x_2$, or $\tau_- < \tau < \tau_+$ and $x_2 < x < x_R$. Then, I_2 becomes

$$I_2 = \int_{x_L}^{x_1} dx \int_{\xi_-}^{\xi_+} \int_{\tau_-}^{\tau_+} \sqrt{1-\xi^2}\, d\xi d\tau \exp\left(-\frac{\sigma(x - x_L)}{\sqrt{1-\xi^2}\,\tau}\right)\left(\Psi_{Lm} - \frac{S_m}{\sigma}\right)$$

$$+ \int_{x_1}^{x_2} dx \int_{\xi_-}^{\xi_+} \int_{\hat{\tau}(x)}^{\tau_+} \sqrt{1-\xi^2}\, d\xi d\tau \exp\left(-\frac{\sigma(x - x_L)}{\sqrt{1-\xi^2}\,\tau}\right)\left(\Psi_{Lm} - \frac{S_m}{\sigma}\right)$$

$$+ \int_{x_1}^{x_2} dx \int_{\xi_-}^{\xi_+} \int_{\tau_-}^{\hat{\tau}(x)} \sqrt{1-\xi^2}\, d\xi d\tau \exp\left(-\frac{\sigma\Delta y}{\sqrt{1-\xi^2}\,\sqrt{1-\tau^2}}\right)\left(\Psi_{Bm} - \frac{S_m}{\sigma}\right)$$

$$+ \int_{x_2}^{x_R} dx \int_{\xi_-}^{\xi_+} \int_{\tau_-}^{\tau_+} \sqrt{1-\xi^2}\, d\xi d\tau \exp\left(-\frac{\sigma\Delta y}{\sqrt{1-\xi^2}\,\sqrt{1-\tau^2}}\right)\left(\Psi_{Bm} - \frac{S_m}{\sigma}\right) .$$

By the assumption made for the ξ variable, I_2 becomes

$$I_2 = g_m\left\{C_{34}\left(\Psi_{Lm} - \frac{S_m}{\sigma}\right) + C_{35}\left(\Psi_{Bm} - \frac{S_m}{\sigma}\right)\right\} , \tag{11}$$

where

$$C_{34} = \int_{x_L}^{x_1} dx \int_{\tau_-}^{\tau_+} d\tau \exp\left(-\frac{\sigma_p(x - x_L)}{\tau}\right) + \int_{x_1}^{x_2} dx \int_{\hat{\tau}(x)}^{\tau_+} d\tau \exp\left(-\frac{\sigma_p(x - x_L)}{\tau}\right) \tag{12}$$

and

$$C_{35} = \int_{x_1}^{x_2} dx \int_{\tau_-}^{\hat{\tau}(x)} d\tau \exp\left(-\frac{\sigma_p \Delta y}{\sqrt{1-\tau^2}}\right) + \int_{x_2}^{x_R} dx \int_{\tau_-}^{\tau_+} d\tau \exp\left(-\frac{\sigma_p \Delta y}{\sqrt{1-\tau^2}}\right) . \tag{13}$$

Meanwhile, the first term of Eq. (5), I_1, becomes

$$I_1 = g_m\, \Delta\mu_m\, \Delta x\, S_m/\sigma . \tag{14}$$

Finally, adding Eq. (14) to Eqs. (6), (8), and (11), and equating them to Eq. (4), we have three equations. Dividing both sides of these equations by $g_m \Delta x \Delta \mu_m$ and rearranging leads to the following relations between the outgoing cone flux on the surface TOP and the incoming cone fluxes on either the surfaces BOTTOM or LEFT, or both:

$$\Psi_{Tm} = \begin{cases} C'_{31}\Psi_{Lm} + (1 - C'_{31})S_m/\sigma & \text{for } \tau_o \leq \tau_- \\ C'_{32}\Psi_{Lm} + C'_{33}\Psi_{Bm} + (1 - C'_{32} - C'_{33})S_m/\sigma & \text{for } \tau_- < \tau_o \leq \tau_+ \\ C'_{34}\Psi_{Lm} + C'_{35}\Psi_{Bm} + (1 - C'_{34} - C'_{35})S_m/\sigma & \text{for } \tau_+ < \tau_o \end{cases} \tag{15}$$

where $C'_{3i} = C_{3i}/\Delta\mu_m \Delta x$ for i = 1, 2, 3, 4, and 5 .

As for the cone flux on the surface RIGHT, relations similar to Eqs. (15) are obtained:

$$\Psi_{Rm} = \begin{cases} D'_{31}\Psi_{Bm} + (1 - D'_{31})S_m/\sigma & \text{for } \rho_o \leq \rho_- \\ D'_{32}\Psi_{Bm} + D'_{33}\Psi_{Lm} + (1 - D'_{32} - D'_{33})S_m/\sigma & \text{for } \rho_- < \rho \leq \rho_+ \\ D'_{34}\Psi_{Bm} + D'_{35}\Psi_{Lm} + (1 - D'_{34} - D'_{35})S_m/\sigma & \text{for } \rho_+ < \rho_o \end{cases} \tag{16}$$

where $\rho_o = \sin(\Delta y/\Delta x)$

$\rho_\pm = \sin(\psi_\pm)$

$\Delta\eta_m = \sin\psi_+ - \sin\psi_-$, and

$D'_{31} = D_{3i}/\Delta y \Delta\eta_m$ for i = 1, 2, 3, 4, and 5 .

To make the formulas more concise, we rewrite Eqs. (15) and (16) in the following way according to Eq. (2.25) in Ref. 1:

$$\Psi_{Tm} = T_{TLm}\Psi_{Lm} + T_{TBm}\Psi_{Bm} + P_{Tm}S_m \tag{17}$$

$$\Psi_{Rm} = T_{RLm}\Psi_{Lm} + T_{RBm}\Psi_{Bm} + P_{Rm}S_m \tag{18}$$

where T_{TLm}, T_{TBm}, T_{RLm}, and T_{RBm} are called the transfer matrix elements and P_{Tm} and P_{Rm} are called the escape matrix elements. These elements are given in Tables 1(a) and (b). As we described in Section 3 of Ref. 1, these elements are sufficient for actual calculations because all other elements are obtained from these by symmetry.

The source term $S(\underline{r},\underline{\Omega},E)$ is given by a summation of Eqs. (2.14) and (2.15) in Ref. 1, and an external source term. Applying the multigroup method and assuming the sources are constant over the mesh cell, we find the source term of the g'th energy group:

$$S_g(\underline{\Omega}) = S_{cg}(\underline{\Omega}) + S_{fg} + Q_g(\underline{\Omega}) \ , \tag{19}$$

where

$$S_{cg}(\underline{\Omega}) = \sum_{h=1}^{G} \int d\Omega' \ \sigma_{sh\to g} \ f(\underline{\Omega}'\to\underline{\Omega}) \ \Psi_g(\underline{\Omega}') \tag{20}$$

and

$$S_{fg} = \frac{1}{4\pi} \chi_g \sum_{h=1}^{G} (\nu\sigma_f)_h \int \Psi_h(\underline{\Omega}') \, d\Omega' \ . \tag{21}$$

In Eq. (20), $f(\underline{\Omega}'\to\underline{\Omega})$ is the probability that a particle in the direction $\underline{\Omega}'$ is scattered into the direction $\underline{\Omega}$, and $\sigma_{sh\to g}$ is the scattering cross section from the h'th to the g'th energy group. In Eq. (21), χ_g is the energy distribution

Table 1(a) Elements of the Transfer and Escape Matrices for the Surface TOP

CASE \ ELEMENTS	T_{TLm}	T_{TBm}	P_{Tm}
$\tau_o \leq \tau_-$	C'_{31}	0	$(1 - C'_{31})/\sigma$
$\tau_- < \tau_o \leq \tau_+$	C'_{32}	C'_{33}	$(1 - C'_{32} - C'_{33})/\sigma$
$\tau_+ < \tau_o$	C'_{34}	C'_{35}	$(1 - C'_{34} - C'_{35})/\sigma$

Table 1(b). Elements of the Transfer and Escape Matrices for the Surface RIGHT

CASE \ ELEMENTS	T_{RLm}	T_{RBm}	P_{Rm}
$\rho_o \leq \rho_-$	0	D'_{31}	$(1 - D'_{31})/\sigma$
$\rho_- < \rho_o \leq \rho_+$	D'_{33}	D'_{32}	$(1 - D'_{32} - D'_{33})/\sigma$
$\rho_+ < \rho_o$	D'_{35}	D'_{34}	$(1 - D'_{34} - D'_{35})/\sigma$

of fission produced neutrons, and $(\nu\sigma_f)_h$ is the number of neutrons produced by a fission reaction times the reaction cross section of the h'th energy group.

The probability function f is expanded by use of spherical harmonic functions in polar coordinates where the direction $\underline{\Omega}'$ is identical to the polar axis. Then, the scattering source term is represented as[3]

$$S_{cg}(\underline{\Omega}) = \sum_{h=1}^{G} \sum_{n=0}^{\infty} (2n + 1)\ \sigma_{shn} \sum_{k=0}^{n} R_n^k(\mu,\psi)\ \Psi_{hn}^k \tag{22}$$

where $$\Psi_{hn}^k = \int_{-1}^{1} d\mu \int_{0}^{\pi} d\psi\ \Psi_h(\mu,\psi)\ R_n^k(\mu,\psi)/2\pi$$

and R_n^k is the spherical harmonic.

In the discrete cones method, we use the following sources averaged over the m'th cone:

$$S_{cgm} = \sum_{h=1}^{G} \sum_{n=0}^{L} (2n + 1)\ \sigma_{shn} \sum_{k=0}^{n} R_n^k(\mu_m,\psi_m)\ \Psi_{hnm}^k\ , \tag{23}$$

$$S_{fgm} = \frac{1}{4\pi}\ \chi_g \sum_{h=1}^{G} (\nu\sigma_f)_h \sum_{m=1}^{MT} \hat{w}_m \Psi_{hm}\ , \tag{24}$$

and $$Q_{gm} = Q_g(\mu_m,\psi_m)\ , \tag{25}$$

where MT = N(N + 2) for the DC_N approximation, (μ_m,ψ_m) is a discrete direction of the EQ_N quadrature set, and Ψ_{hnm}^k is given by

$$\Psi_{hnm}^k = \sum_{m=1}^{MT} \hat{w}_m R_n^k(\mu_m,\psi_m)\ \Psi_{hm}\ . \tag{26}$$

In Eq. (23), the summation with respect to n is stopped at n = L, and the approximation is called the P_L approximation. Ψ_{hm} is called the cone flux. The solar flux, ϕ, is given by

$$\phi = \sum_{m=1}^{MT} \hat{w}_m \Psi_{hm} . \tag{27}$$

For Eqs. (17) and (18) to find the outgoing flux Ψ_{Tm} and Ψ_{Rm}, we must know the incoming fluxes Ψ_{Bm} and Ψ_{Lm} and the source term S_m; however, S_m depends on the cone flux Ψ_m averaged over a spatial mesh cell. Hence, Ψ_m must be calculated in some way. In actual calculations, S_m is computed by using the Ψ_m of the previous inner iteration.

To find the cell cone flux Ψ_m, we first proposed a flux averaged over the two outgoing cone fluxes and the two incoming cone fluxes of the m'th cone:

$$\Psi_m = \frac{1}{4} \left(\Psi_{Lm} + \Psi_{Bm} + \Psi_{Rm} + \Psi_{Tm} \right) . \tag{28}$$

Our numerical experiences, however, show that the use of Eq. (28) results in a slow convergence of the inner iteration; it requires twice or more the inner iterations compared to the discrete ordinates method (TWOTRAN-II).

As is known, the coarse mesh rebalancing technique for acceleration of convergence demands particle balance in a specific spatial domain, and the technique has been successfully applied.[3] This suggested enforcing particle balance in a mesh cell and a cone so that convergence is accelerated in the discrete cones method.

Transferring the total scattering term $\sigma_t \Psi$ to the right-hand side in Eq. (2.16) in Ref. 1, and defining the current by $\underline{j} = \underline{\Omega}\Psi$, we have

$$\underline{\nabla}\cdot\underline{j}(\underline{r},\underline{\Omega}) = S(\underline{r},\underline{\Omega}) - \sigma_t(\underline{r})\ \Psi(\underline{r},\underline{\Omega}) \ , \tag{29}$$

where the subscript g is omitted. This equation states the particle conservation at a spatial point, $\underline{r}$, in a direction, $\underline{\Omega}$. To apply Eq. (29) to a mesh cell D_i, we integrate it over the mesh cell D_i and the m'th cone. By the divergence theorem: $\int_{D_i} \underline{\nabla}\cdot\underline{j}\ d\underline{r} = \int_{\partial D_i} \underline{j}\cdot\underline{n}\ dA$, we have

$$\iint_{\Delta\Omega_m} \int_{\partial D_i} \underline{j}\cdot\underline{n}\ dA d\underline{\Omega} = \iint_{\Delta\Omega_m} \int_{D_i} (S - \sigma_t\Psi)\ d\underline{r}d\underline{\Omega} \ . \tag{30}$$

Let us consider a mesh cell as shown in Fig. 1. Assuming $S - \sigma_t\Psi$ is constant over the mesh cell D_i and the m'th cone $\Delta\Omega_m$, and Ψ is constant on each boundary surface: TOP, BOTTOM, RIGHT, and LEFT, and the m'th cone, we find

$$FT_m + FR_m + FL_m + FB_m = \Delta x\Delta y\hat{w}_m(S_m - \sigma_t\Psi_m) \ , \tag{31}$$

where

$$FT_m = \Delta x\left(\iint_{\Delta\Omega_m} \underline{\Omega}\cdot\underline{n}_T\ d\underline{\Omega}\right)\ \Psi_{Tm} \ ,$$

$$FR_m = \Delta y\left(\iint_{\Delta\Omega_m} \underline{\Omega}\cdot\underline{n}_R\ d\underline{\Omega}\right)\ \Psi_{Rm} \ ,$$

$$FL_m = \Delta y\left(\iint_{\Delta\Omega_m} \underline{\Omega}\cdot\underline{n}_L\ d\underline{\Omega}\right)\ \Psi_{Lm} \ ,$$

and

$$FB_m = \Delta x\left(\iint_{\Delta\Omega_m} \underline{\Omega}\cdot\underline{n}_B\ d\underline{\Omega}\right)\ \Psi_{Bm} \ .$$

Solving Eq. (31) for Ψ_m results in a formula of the cone flux Ψ_m:

$$\Psi_m = \frac{1}{\sigma_t}\left(S_m - \frac{FT_m + FR_m + FL_m + FB_m}{\Delta x\Delta y\hat{w}_m}\right) \ . \tag{32}$$

As we will see later, this expression, in fact, accelerates the convergence of the inner iterations.

3. CALCULATION OF THE TRANSFER AND ESCAPE MATRIX ELEMENTS

In this section, we perform integrations of the transfer matrix elements T_{TLm}, T_{TBm}, T_{RLm}, and T_{RBm}, and the escape matrix elements P_{Tm} and P_{Rm}; equivalently, we must calculate the constants C_{3i} and D_{3i} for $i = 1$ to 5.

By integrating Eq. (7) with respect to x, it becomes

$$C_{31} = \frac{\tau_+^2 - \tau_-^2}{2\sigma_p} - \frac{1}{\sigma_p} \int_{\tau_-}^{\tau_+} d\tau \, \tau \exp\left(-\frac{\sigma_p \Delta x}{\tau}\right) .$$

The second term is converted by the following formula of integration:

$$\int_a^b d\mu \, \mu \exp\left(-\frac{\alpha}{\mu}\right) = \frac{1}{2}(b^2 - \alpha b) \exp\left(-\frac{\alpha}{b}\right) - \frac{1}{2}(a^2 - \alpha a) \exp\left(-\frac{\alpha}{a}\right) + \frac{\alpha^2}{2}\left\{E_1\left(\frac{\alpha}{b}\right) - E_1\left(\frac{\alpha}{a}\right)\right\} , \tag{33}$$

where the exponential integral $E_1(x)$ is defined by[4]

$$E_1(x) = \int_x^\infty \frac{e^{-t}}{t} dt ,$$

and α is a positive constant. Applying Eq. (33) to the second term of C_{31} results in

$$C_{31} = \frac{\tau_+^2 - \tau_-^2}{2\sigma_p} - \frac{1}{2\sigma_p}(\tau^2 - \sigma_p \Delta x \tau_+) \exp\left(-\frac{\sigma_p \Delta x}{\tau_+}\right) + \frac{1}{2\sigma_p}(\tau_-^2 - \sigma_p \Delta x \tau_-) \exp\left(-\frac{\sigma_p \Delta x}{\tau_-}\right) + \frac{\sigma_p (\Delta x)^2}{2}\left\{E_1\left(\frac{\sigma_p \Delta x}{\tau_-}\right) - E_1\left(\frac{\sigma_p \Delta x}{\tau_+}\right)\right\} . \tag{34}$$

As for the second term of Eq. (9), we must first integrate it with respect to τ because the integral limit $\hat{\tau}(x)$ is a function of x. But doing so leads to exponential functions whose arguments contain $\hat{\tau}(x)$. Integrating it with respect to x is very complicated. In order to simplify the integral, we look at the integral limits from a different point of view. The integral limits are illustrated in Fig. 2. If we first integrate with respect to x, the second term becomes

$$\int_{\tau_-}^{\tau_o} d\tau \int_{x_1}^{x(\tau)} dx \exp\left(-\frac{\sigma_p(x - x_L)}{\tau}\right) + \int_{\tau_-}^{\tau_+} d\tau \int_{x_1}^{x_R} dx \exp\left(-\frac{\sigma_p(x - x_L)}{\tau}\right) ,$$

where $x(\tau) = x_L + \tau\Delta y/\sqrt{1 - \tau^2}$ and $\tau_o = \Delta x/\sqrt{\Delta x^2 + \Delta y^2}$. Performing the integration with respect to x leads to

$$\frac{1}{\sigma_p}\int_{\tau_-}^{\tau_+} d\tau\ \tau \exp\left(-\frac{\sigma_p(x_1 - x_L)}{\tau}\right) - \frac{1}{\sigma_p}\int_{\tau_-}^{\tau_o} d\tau\ \tau \exp\left(-\frac{\sigma_p \Delta y}{\sqrt{1 - \tau^2}}\right)$$

$$- \frac{1}{\sigma_p}\int_{\tau_o}^{\tau_+} d\tau\ \tau \exp\left(-\frac{\sigma_p \Delta x}{\tau}\right) .$$

We apply the formula (33) and the following equation (35) to the above expression:

$$\int_a^b d\mu\ \mu \exp\left(-\frac{\alpha}{\sqrt{1 - \mu^2}}\right) = -\frac{1}{2}\left(1 - b^2 - \alpha\sqrt{1 - b^2}\right)\exp\left(-\frac{\alpha}{\sqrt{1 - b^2}}\right)$$

$$+ \frac{1}{2}\left(1 - a^2 - \alpha\sqrt{1 - a^2}\right)\exp\left(-\frac{\alpha}{\sqrt{1 - a^2}}\right) + \frac{1}{2}\left\{E_1\left(\frac{\alpha}{\sqrt{1 - a^2}}\right)\right. \qquad (35)$$

$$\left. - E_1\left(\frac{\alpha}{\sqrt{1 - b^2}}\right)\right\} .$$

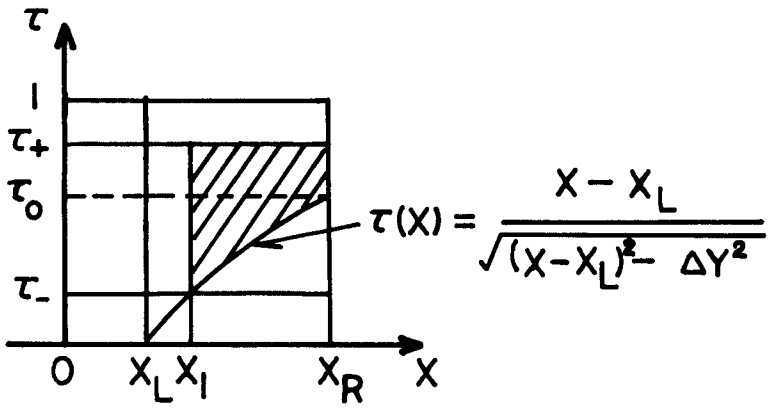

Fig. 2 The integral limit for the second term of Eq. 19.

As for the first term of Eq. (9), we first integrate it with respect to x to find

$$\frac{\tau_+^2 - \tau_-^2}{2\sigma_p} - \frac{1}{\sigma_p}\int_{\tau_-}^{\tau_+} d\tau\ \tau \exp\left(-\frac{\sigma_p(x_1 - x_L)}{\tau}\right) . \tag{36}$$

Finally, we obtain the following expression for C_{32}:

$$\begin{aligned} C_{32} = {} & \frac{\tau_+^2 - \tau_-^2}{2\sigma_p} - \frac{1}{2\sigma_p}\exp\left(-\frac{\sigma_p \Delta x}{\tau_+}\right)\left(\tau_+^2 - \sigma_p \Delta x \tau_+\right) + \frac{1}{2\sigma_p}\exp\left(-\frac{\sigma_p \Delta x}{\tau_o}\right) \\ & \times \left(\tau_o^2 - \sigma_p \Delta x \tau_o\right) - \frac{\sigma_p \Delta x^2}{2}\left\{E_1\left(\frac{\sigma_p \Delta x}{\tau_+}\right) - E_1\left(\frac{\sigma_p \Delta x}{\tau_o}\right)\right\} \\ & + \frac{1}{2\sigma_p}\exp\left(-\frac{\sigma_p \Delta y}{\sqrt{1 - \tau_o^2}}\right)\left(1 - \tau_o^2 - \sigma_p \Delta y \sqrt{1 - \tau_o^2}\right) - \frac{1}{2\sigma_p}\exp\left(-\frac{\sigma_p \Delta y}{\sqrt{1 - \tau_o^2}}\right) \\ & \times \left(1 - \tau_-^2 - \sigma_p \Delta y \sqrt{1 - \tau_-^2}\right) - \frac{\sigma_p \Delta y^2}{2}\left\{E_1\left(\frac{\sigma_p \Delta y}{\sqrt{1 - \tau_-^2}}\right) - E_1\left(\frac{\sigma_p \Delta y}{\sqrt{1 - \tau_o^2}}\right)\right\} . \end{aligned} \tag{37}$$

In the same way, we find the following expressions for the constants C_{33}, C_{34}, and C_{35}.

$$\begin{aligned} C_{33} = {} & \Delta x \int_{\tau_-}^{\tau_o} d\tau \exp\left(-\frac{\sigma_p \Delta y}{\sqrt{1 - \tau^2}}\right) + \sqrt{1 - \tau_o^2}\ \Delta y \exp\left(-\frac{\sigma_p \Delta y}{\sqrt{1 - \tau_o^2}}\right) \\ & - \sqrt{1 - \tau_-^2}\ \Delta y \exp\left(-\frac{\sigma_p \Delta y}{\sqrt{1 - \tau_-^2}}\right) + \sigma_p \Delta y^2 \left\{E_1\left(\frac{\sigma_p \Delta y}{\sqrt{1 - \tau_-^2}}\right) - E_1\left(\frac{\sigma_p \Delta y}{\sqrt{1 - \tau_o^2}}\right)\right\} \end{aligned} \tag{38}$$

$$C_{34} = \frac{\tau_+^2 - \tau_-^2}{2\sigma_p} + \frac{1}{2\sigma_p}\exp\left(-\frac{\sigma_p \Delta y}{\sqrt{1-\tau_+^2}}\right)\left(1 - \tau_+^2 - \sigma_p \Delta y\sqrt{1-\tau_+^2}\right) \tag{39}$$

$$- \frac{1}{2\sigma_p}\exp\left(-\frac{\sigma_p \Delta y}{\sqrt{1-\tau_-^2}}\right)\left(1 - \tau_-^2 - \sigma_p \Delta y\sqrt{1-\tau_-^2}\right)$$

$$+ \frac{\sigma_p \Delta y^2}{2}\left\{E_1\left(\frac{\sigma_p \Delta y}{\sqrt{1-\tau_+^2}}\right) - E_1\left(\frac{\sigma_p \Delta y}{\sqrt{1-\tau_-^2}}\right)\right\}$$

$$C_{35} = \Delta x \int_{\tau_-}^{\tau_+} d\tau \exp\left(-\frac{\sigma_p \Delta y}{\sqrt{1-\tau^2}}\right) + \sqrt{1-\tau_+^2}\ \Delta y \exp\left(-\frac{\sigma_p \Delta y}{\sqrt{1-\tau_+^2}}\right) \tag{40}$$

$$- \sqrt{1-\tau_-^2}\ \Delta y \exp\left(-\frac{\sigma_p \Delta y}{\sqrt{1-\tau_-^2}}\right) + \sigma_p \Delta y^2\left\{E_1\left(\frac{\sigma_p \Delta y}{\sqrt{1-\tau_-^2}}\right) - E_1\left(\frac{\sigma_p \Delta y}{\sqrt{1-\tau_+^2}}\right)\right\}.$$

The constants D_{3i} ($i = 1, 2, \ldots, 5$) of the transfer matrix elements for the surface RIGHT are easily obtained by replacing Δx, Δy, τ_+, τ_-, and τ_o in Eqs. (34), (37), (38), (39), and (40) by Δy, Δx, ρ_-, ρ_+, and ρ_o, respectively.

There are two integrals left in the above formulas. The exponential integral $E_1(x)$ is evaluated by means of approximate functions given by 5.1.53 and 5.1.56 in Ref. 5. For convenience, the expressions are reproduced as follows.

For $0 < x < 1$

$$E_1(x) = -\ln x + a_o + a_1 x + a_2 x^2 + a_3 x^3 + a_4 x^4 + a_5 x^5 + \varepsilon(x) \tag{41}$$

where the error $|\varepsilon(x)| < 2 \times 10^{-7}$ and

$$a_0 = -0.57721566,\ a_1 = 0.99999193,\ a_2 = -0.24991055,$$
$$a_3 = 0.05519968,\ a_4 = -0.00976004,\ a_5 = 0.00107857\ .$$

For $1 \leq x < \infty$

$$xe^x E_1(x) = \frac{x^4 + a_1x^3 + a_2x^2 + a_3x + a_4}{x^4 + b_1x^3 + b_2x^2 + b_3x + b_4} + \varepsilon(x)\ , \qquad (42)$$

where the error $|\varepsilon(x)| < 2 \times 10^{-8}$ and

$$a_1 = 8.5733287401, \qquad b_1 = 9.5733223454$$
$$a_2 = 18.0590169730, \qquad b_2 = 25.6329561486$$
$$a_3 = 8.6437608925, \qquad b_3 = 21.0996530827$$
$$a_4 = 0.2677737343, \qquad b_4 = 3.9584969228$$

Another integral, $\int_a^b dx\ \exp\left(-\alpha/\sqrt{1 - x^2}\right)$, is numerically integrated by using the 8'th order Gaussian quadrature formula given by Ref. 6.

4. PROGRAMS DCTRAN-II AND DCTRAN-X

The discrete cones method developed in the preceding sections was implemented in the discrete ordinates code TWOTRAN-II.[3] The code is available through the National Magnetic Fusion Energy Computer Center at Livermore, California.

The following five subprograms are added to the TWOTRAN-II program:

EQNGEN - contains the equal weight quadrature set EQ_N for $2 \leq N \leq 16$; the values are taken from Ref. 7. The subprogram SNCON built into TWOTRAN is not used in the present program.

QUADSET - calculates the discrete cone boundaries.

COEF - calculates the transfer and escape matrix elements.

AAF - evaluates the exponential integral in the transfer and escape matrix elements by using approximations described in Section 3.

GINT - evaluates the integral: $\int_a^b d\mu \exp(-\alpha/\sqrt{1-\mu^2})$ by using the 8'th order Gaussian quadrature.

In addition to these new subprograms, two subprograms IN and OUT in TWOTRAN-II were completely changed. The new subprograms apply Eqs. (15), (16), and (32) to find the cell edge fluxes and the cell average fluxes in sweeping the spatial mesh cells. The negative flux fix-up scheme is discarded. The new program is named DCTRAN-II, and it runs only on the CDC-7600. The DCTRAN-II calls the subprogram COEF in a subprogram GRIND21 of overlay 2.

As we described in Ref. 1, the discrete cones method was successfully applied to a solution in a void. Hence, by applying the discrete cones method to both a void and a non-void, a new program, DCTRAN-X, was created. In addition to the above five subprograms, the program has a subprogram VOID, which calculates the transfer and escape matrix elements of a void. This program runs on the CRAY-1 computer. The structure of DCTRAN-X is shown in Table 2.

At present, the DCTRAN-X program is available only for problems in X-Y geometry. An extension of the method to other geometries seems extremely complicated and is left for the future.

5. NUMERICAL RESULTS

The program DCTRAN-X was run on the CRAY-1 computer to test the discrete cones method. The method is examined from two points of view: accuracy and computing efficiency. The accuracy is categorized into two points: one of them is the accuracy of physical quantities obtained by integrating a function

Table 2. Structure of the DCTRAN-X Program

OVERLAY(0,0)
DCTRAN[2)]
1 MONITOR
2 ERROR
3 CLEAR
4 MPLY
5 WRITE
6 ECHECK
7 DUMPER
8 PCMBAL
9 REED
10 RITE

OVERLAY(1,0)
INPUT1
1 LOAD
2 INPT11[2)]
a DUMPRD
3 INPT12
a CSPREP
b IFINXS
4 INPT13
a READQF
b IFINQF
5 INPT14[2)]
a EQNCON[1)]
b IFINSN
c PNGEN
d QUADSET
6 INPT15
a CSMESH
b MAPPER

OVERLAY(2,0)
GRIND2
1 REBAL
2 GRIND21[2)]
a COEF[1)]
b AAF[1)]
c GINT[1)]
d VOID[1)]
e INITAL
f INITQ
g FISCAL
3 GRIND22
a OUTER
b INNER[2)]
c IN[2)]
d OUT[2)]
e SETBC
f STORAF
g SAVEAF
h GSUMS
4 GRIND23
a TESTS
b NEWPAR

OVERLAY(3,0)
OUTPUT3
1 OUTPT31
a FINAL
2 OUTPT32
a EDCALL
b GENFLO
c EDITOR
d EDMAP
3 IFOUT
a IFRITE

1) These subprograms are newly added to the TWOTRAN-II program.

2) These subprograms are modified.

over a certain spatial domain, D; these quantities are defined by $\int_D f(\underline{r})\phi(\underline{r})\, dr$, where $f(\underline{r})$ is a response function such as the absorption cross section, and $\phi(\underline{r})$ is the scalar flux. Another is the accuracy of the spatial distribution of the scalar flux, i.e., how much the ray effect is mitigated.

In terms of numerical analysis, the first accuracy corresponds to the L^2 error defined by $\|F\|_2 = (\int_D F^2(\underline{r})\, d\underline{r})^{1/2}$, and the second corresponds to the L^∞ error defined by $\|F\|_\infty = \max_{\underline{r}\in D} F(\underline{r})$.

PROBLEM 1. One Group Problem

This problem is solved to see how much the ray effects are mitigated by the discrete cones method. The system consists of an isotropic source distributed uniformly and a pure absorber surrounding the source. The geometry and the cross sections are shown in Fig. 3.

The problem is solved for one energy group and isotropic scattering materials by the S_8 and S_{16} approximations (TWOTRAN-II), and the DC_8 approximation (DCTRAN-X). The spatial domain is partitioned into 16 by 16 mesh cells for all cases. The size of a mesh cell is 1/2 mfp.

The scalar flux distributions along the right edge of the system are plotted in Fig. 4. The distribution is expected to be a cosine-like curve whose maximum is at x = 0. The DC_8 solution satisfies this requirement; meanwhile, the S_8 and S_{16} solutions show oscillatory behavior due to the ray effects. As a whole, the scalar flux of the DC_8 solution is somewhat larger than the S_8 and S_{16} solutions. The cause of such a discrepancy will be further investigated in the following examples.

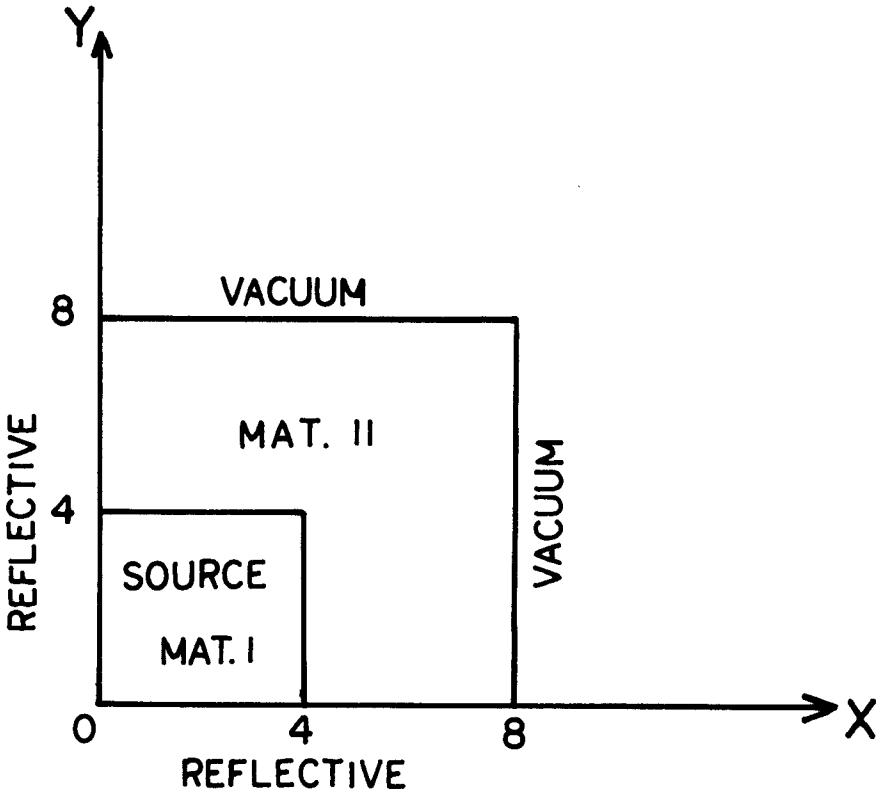

	σ_a	σ_t	σ_s
MAT. I	0.75	1.0	0.25
MAT. II	1.0	1.0	0.0

Fig. 3 Geometry and cross sections for Problem 1.

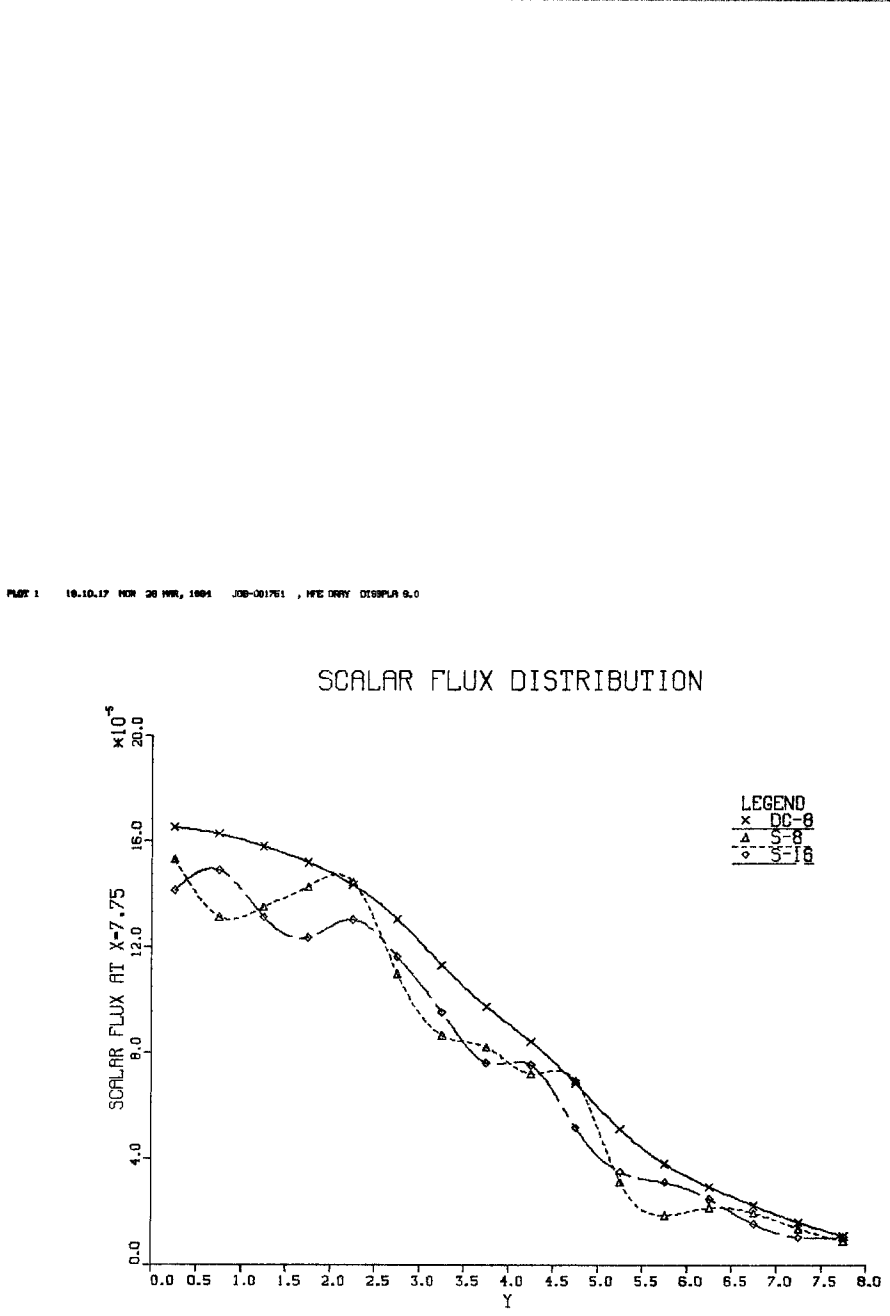

Fig. 4 The scalar flux distribution at x = 7.75 for Problem 1.

PROBLEM 2. One Group Problem

The domain of the problem consists of only one material and an isotropic source is uniformly distributed in a square. The geometry and the cross sections are shown in Fig. 5. The net leakage from the system and the total absorption in the system are calculated by varying the order of the DC_N approximation and the number of spatial mesh cells.

The results are shown in Table 3. On the same table we list the S_{16} solution for 20 times 20 mesh cells as a reference solution; 4/30 mfp is chosen as the size of the square mesh cell so that sufficient accuracy is achieved by the calculation. Observing Table 3, we find that the net leakage of the DC_N solutions is larger than the S_{16} solution when the spatial domain is roughly partitioned; on the other hand, the total absorption of the DC_N solutions is smaller than the S_{16} solution. As the mesh is refined, the net leakage decreases and the total absorption increases. For a certain spatial partitioning, the best accuracy is achieved. However, refining the mesh further increases the errors. As shown in columns for the DC_4 approximations, the solution does not seem to converge to the exact value even if extremely fine mesh cells are used.

The results suggest the following expression for the error of the cell average cone flux Ψ:

$$\Psi = \Psi^e + \varepsilon_s + \varepsilon_a \qquad \text{for } \varepsilon_s < 0 \text{ and } \varepsilon_a > 0 \,, \tag{43}$$

where Ψ^e is the exact cell average cone flux, ε_s is the error due to the spatial discretization, and ε_a is the error due to the angle discretization. As the space and angle are partitioned further, $|\varepsilon_s| \to 0$ and $|\varepsilon_a| \to 0$.

Table 3. Dependence of Accuracy on Mesh Size for Problem 2

TWOTRAN-II

	NET LEAKAGE	ABSORPTION
S_2, 20 x 20	4.0133681E-01	5.9866317E-01
S_{16}, 20 x 20	4.0101376E-01	5.9898766E-01

DCTRAN-X

(DC24FEB4)	NET LEAKAGE	ABSORPTION
DC_2, 2 x 2	4.163692E-01	5.8363147E-01
4 x 4	3.8969266	6.1030741
8 x 8	3.7153841	6.2846166
16 x 16	3.6030616	6.3969390
DC_4, 2 x 2	4.190945	5.8090606
4 x 4	4.0071642	5.9928365
8 x 8	3.9071642	6.0923310
16 x 16	3.8546140	6.1453867
32 x 32	3.8500853	6.1499153
64 x 64	3.8125000	6.1875006
DC_8, 2 x 2	4.2368633	5.7631364
4 x 4	4.0864249	5.9135841
8 x 8	4.0162278	5.9837734
16 x 16	3.9834244	6.0165769
DC_{16}, 2 x 2	4.2532252	5.7467720
4 x 4	4.1121553	5.8878535
8 x 8	4.0488300	5.9511703
16 x 16	4.0202063	5.9797940

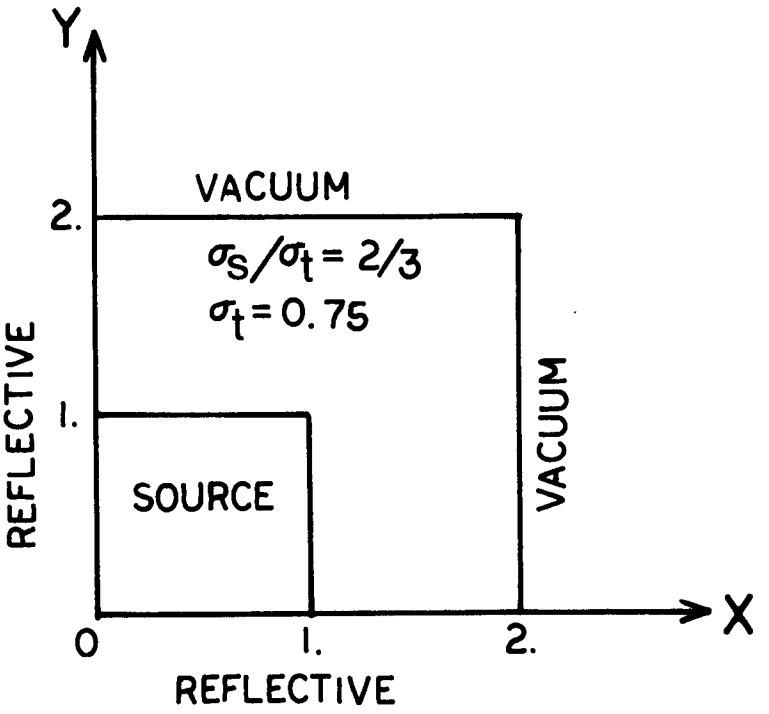

Fig. 5 Geometry for Problem 2.

The total absorption in a domain is given by $\sum_i \sigma_{ai} \sum_m \psi_{mi}$, where i denotes the i'th mesh cell and m denotes the m'th cone. Hence, a smaller absorption implies a smaller cell average cone flux. Since the numerical scheme is formulated so that the particles in a system are conserved, a smaller absorption also implies a larger net leakage. As a result, Eq. (43) exactly represents the numerical behavior of the DC_N solutions given in Table 3.

In conclusion, there is an optimum mesh for an order of the DC_N approximation to achieve the best accuracy of integrated quantities. Detailed numerical analyses are required to do such an optimization.

PROBLEM 3. One Group Problem

This problem is popular in papers dealing with the problem of the ray effects. The spatial domain consists of two materials and an isotropic source as illustrated in Fig. 6. Since there is a localized source and a localized high absorber, this problem is difficult to solve by the discrete ordinates method.

For the present solution, the spatial domain is partitioned into 30 times 30 mesh cells. The scalar flux distributions along the right edge of the domain are plotted for the DC_8, S_8, and S_{16} solutions as well as a solution by the Monte Carlo code MCNP.[8] As seen in Fig. 7 the DC_8 solution is superior to both the S_8 and S_{16} solutions. Table 4 shows the central processor unit time (CPU) in seconds, the number of inner iterations required to achieve the accuracy of 1.0×10^{-4}, the memory size required by the calculations, and the total absorption by material 2. On this table, a true number of memory elements is given by a summation of SCM and LCM. If the orders of the DC_N and S_N approximations are the same, the DC_N calculation requires more memory than the S_N calculation because the former must store the transfer and

Table 4. Computing Time, Memory, and Absorption for Problem 3

	ltss (sec)	CPU (sec)	# of Inner Iterations	Memory SCM	Memory LCM	Absorption at Mat. 2
TWOTRAN-II						
S_8	7.679	5.185	8	7386	7274	3.2996E-3 +4.34%
S_{16}	17.027	16.791	8	10912	7274	3.1623E-3 ±0%
DCTRAN-X (DC24FEB4)						
DC_6	7.119	4.307	8	7058	7466	3.1049E-3 (-1.82%)
DC_8	8.664	6.669	8	7760	7594	3.1249E-3 (-1.18%)
DC_{16}	22.068	22.014	8	12248	8426	3.1164E-3 (-1.45%)

* All the cases were run on CRAY-1.

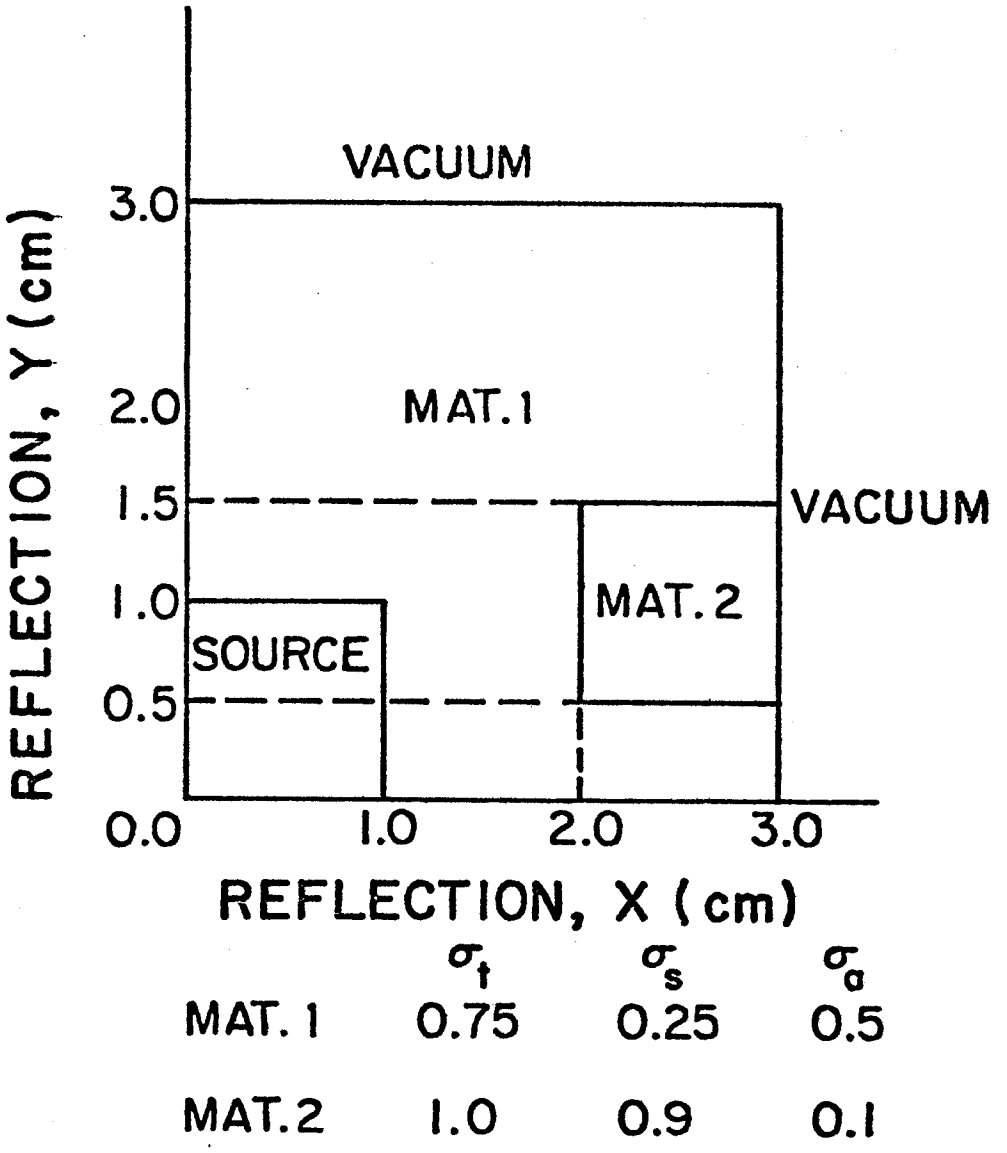

Fig. 6 Geometry and cross sections for Problem 3.

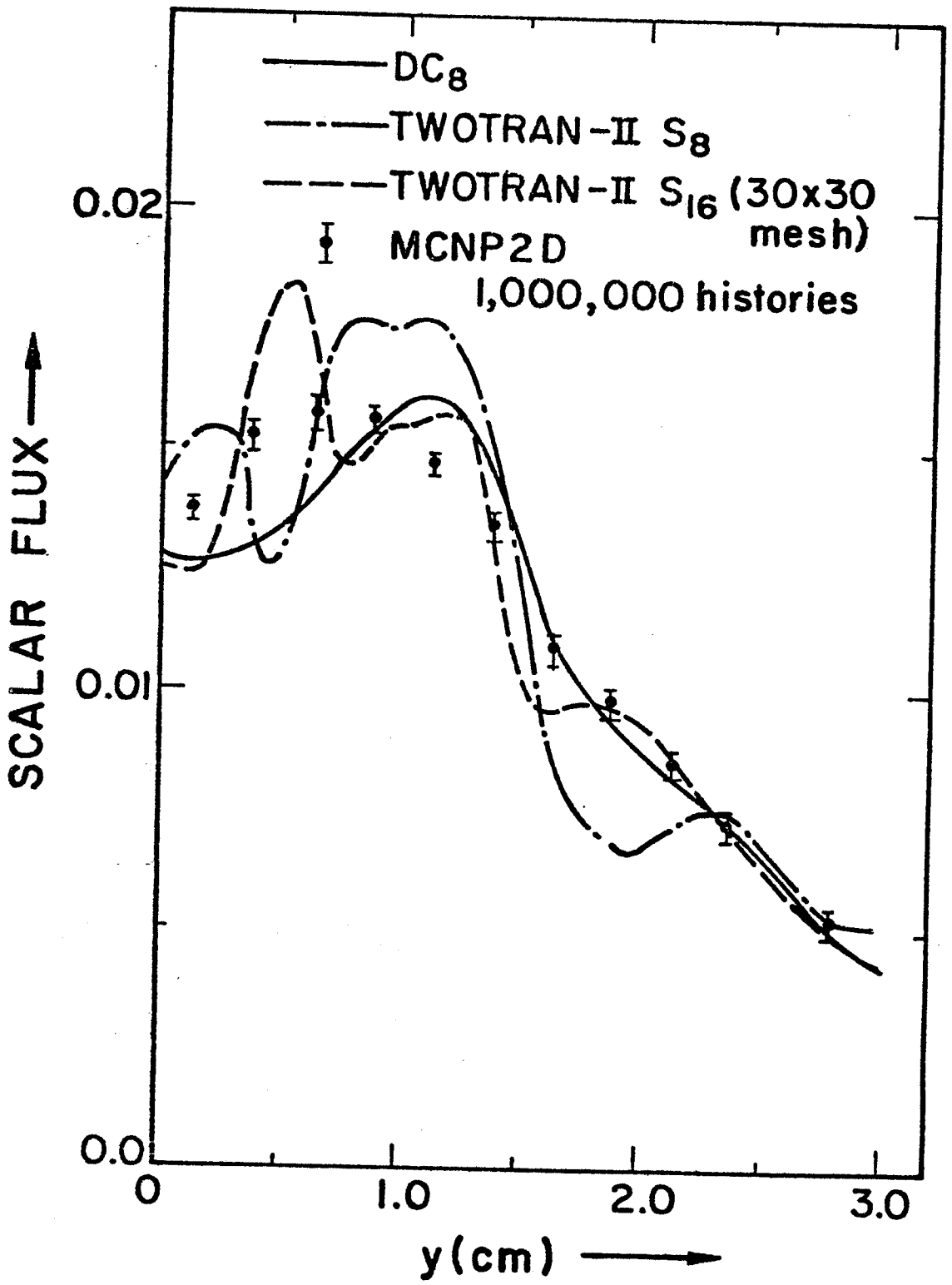

Fig. 7 Scalar flux distribution along the right boundary for Problem 3.

escape matrix elements and the DC_N solution consumes 20 ~ 30% more CPU time even if it requires the same number of inner iterations as the S_N solution. If we believe that the absorption of the S_{16} solution is exact, the DC_8 solution has 2.28% error; meanwhile, the S_8 solution has 4.34% error. Hence, we can conclude the accuracy of the DC_8 solution is sufficient for the integrated value.

PROBLEM 4. 3-Group Eigenvalue Problem

This problem is taken from Ref. 9. The system and the cross sections are shown in Fig. 8 and Table 5(a), respectively. A series of calculations are performed by varying the number of spatial mesh cells as shown in Table 5(c). The multiplication factor, k_{eff}, is calculated. Table 5(b) shows k_{eff} and the CPU time for the S_8 and DC_8 solutions. The errors listed below k_{eff} are calculated by comparing the solution with the S_8 solution of Case 4.

PROBLEM 5. One Group Problem Containing a Void

If a system consists of a void, a highly absorbing material, and a localized source, it is extremely difficult to accurately solve by the discrete ordinates method because of the ray effects. Such a sample problem is solved by the use of the S_8, S_{16}, and DC_8 approximations. The system is illustrated in Fig. 9.

The scalar flux distributions at the right edge of the system are plotted in Fig. 10. For reference, a MCNP solution is also shown. A strong mitigation of the ray effects by the DC_8 approximation is observed; meanwhile, even the S_{16} solution is much worse than the DC_8 solution. Although the improvement by the DC_N method is impressive, it is worth noting that the scalar flux near the x axis is still half of the MCNP solution. Hence, if a more

Table 5(a). Group Cross Sections for Problem 4

Region	Group	χ	$\nu\sigma_t$	σ_T	σ_{gg}	$\sigma_{g-1\to g}$	$\sigma_{g-2\to g}$
I	1	0.7	0.0524	0.1440	0.0871	0	0
I	2	0.2	0.01	0.2591	0.2486	0.0453	0
I	3	0.1	0.006	0.4062	0.3883	0.0387	0.0001
II	1	0	0	0.1	0	0	0
II	2	0	0	0.3	0	0	0
II	3	0	0	5.0	0	0	0
III	1	0	0	0.2163	0.1760	0	0
III	2	0	0	0.3255	0.3236	0.0399	0
III	3	0	0	1.1228	0.9328	0	0

Table 5(b). Computing Time and Eigenvalues for Problem 4

CASE	TWOTRAN-II (S_8)		DCTRAN-X (DC_8)	
	k_{eff}	CPU (sec)	k_{eff}	CPU (sec)
1, 7 x 6	0.59279(-1.28%)	16.717	0.56638(-5.68%)	19.812
2, 14 x 12	0.59869(-0.298%)	69.064	0.59712(-0.560%)	86.362
3, 28 x 24	0.60012(-0.0600%)	274.657	0.61191(+1.90%)	351.191
4, 56 x 48	0.60048	1095.527		

Table 5(c). Number of Fine Mesh Cells of Subregions

REGION / CASE	X-Direction			Y-Direction	
	I	II	III	I, II	III
1	3	1	3	3	3
2	6	2	6	6	6
3	12	4	12	12	12
4	24	8	24	24	24

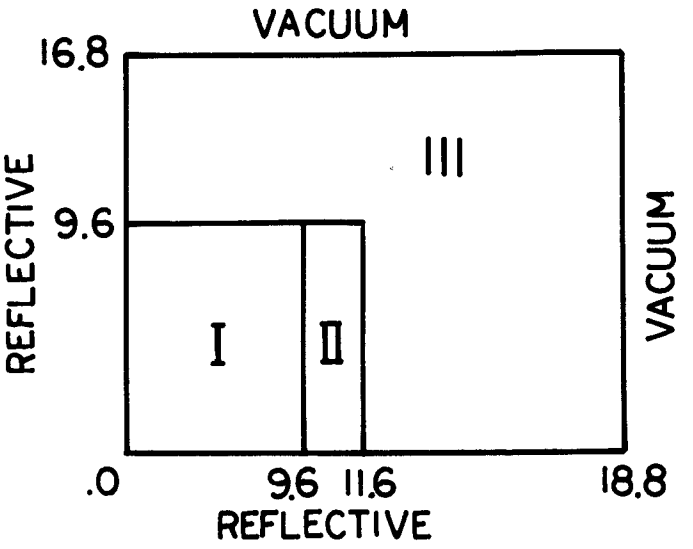

Fig. 8 Geometry for Problem 4.

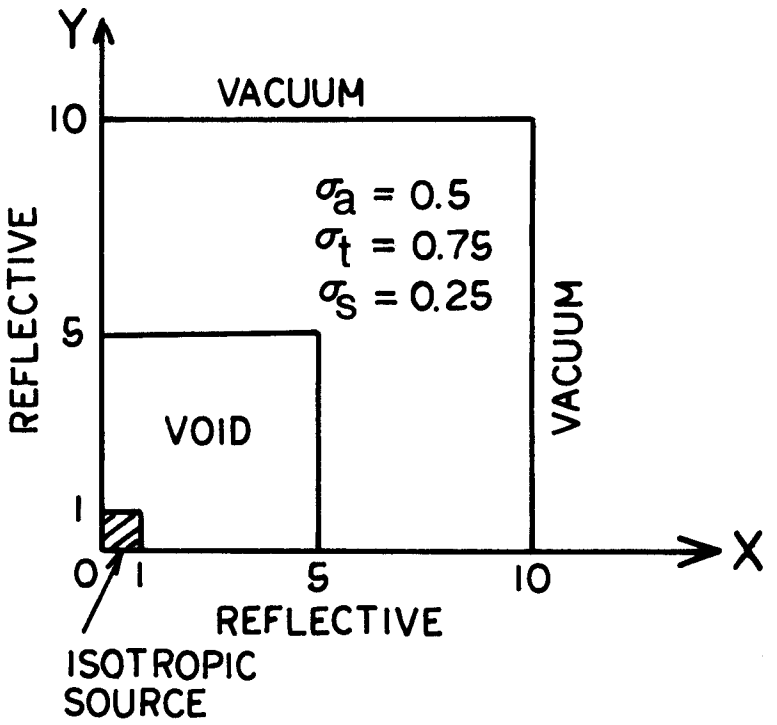

Fig. 9 Geometry and cross sections for Problem 5.

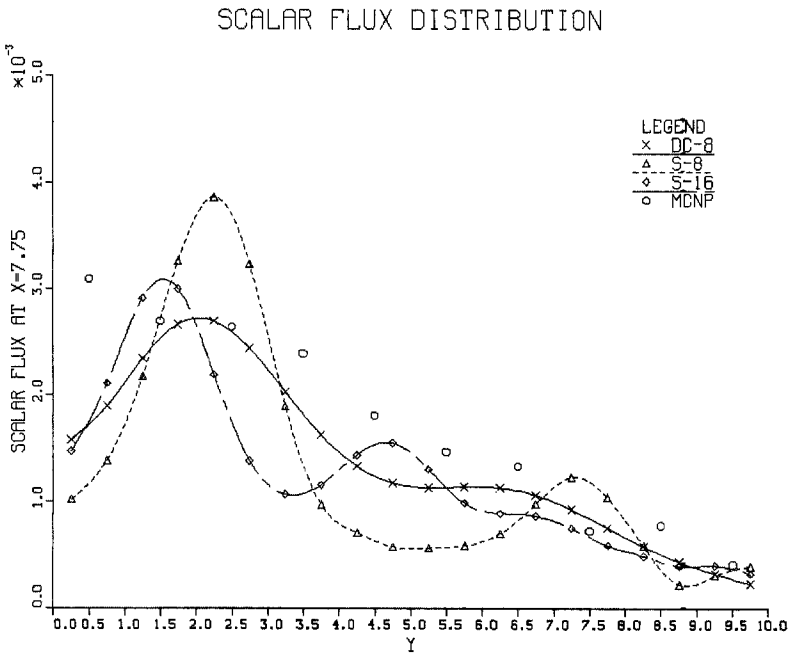

Fig. 10 Scalar flux distribution at x = 7.75 for Problem 5.

accurate solution is required near the x axis, a different method must be used for this problem. As for computing time, see Table 6.

PROBLEM 6. One Group Eigenvalue Problem Containing a Void

This one-group eigenvalue problem is taken from a recent review paper.[10] The system shown in Fig. 11 models a melted core of a fission reactor after an accident. The problem is solved by the S_8 and DC_8 approximations for two spatial partitions: 10 x 20 and 4 x 50 mesh cells. The mean free path (mfp) of the fuel region is smaller than that of the melted core region, and the mean free path of the former is 2.653 cm. The interval in the y direction of the first partition is nearly equal to the mean free path of the fuel region; in contrast, the interval in the y direction of the second partition is 2/5 mfp. The intervals in the x direction of the two partitions are much shorter than the mean free path. The effective multiplication factors, k_{eff}, the number of total inner iterations required to achieve 1.0×10^{-6} for the error of convergence, and the CPU time in seconds are shown in Table 7. The error of k_{eff} is computed by comparing it with k_{eff} calculated by McCoy, who used a quadrature set specially chosen for this problem in the S_N calculations.[10]

The error of the DC_8 solution for the 10 x 20 mesh cells is larger than that of the S_8 solution; meanwhile, the former is smaller than the latter for the 4 x 50 mesh cells. The number of total inner iterations is somewhat reduced by the DC_N method, but the CPU time increases by 20 ~ 40%.

In conclusion, the results demonstrate that the DC_N method works well for eigenvalue problems containing a void if the spatial domain is partitioned so that the interval of mesh cells is much smaller than the mean free path of non-void regions.

Table 6. The Computing Time for Problem 5

Method	CPU (seconds)	Number of Inner Iterations
DC_8	3.379 (1.25)	9
S_8	2.701 (1.0)	9
S_{16}	8.595 (3.18)	9
MCNP	43 minutes on CDC-7600, 200,000 histories	

Table 7. Eigenvalue and the CPU Time for Problem 6

	k_{eff}	No. of Inner Iterations	CPU (seconds)	Mesh
DC_8	0.75779(-4.048%)	341	62.531	10 x 20
	0.78521(-0.5761%)	413	78.416	4 x 50
S_8	0.79802(+1.0459%)	436	52.733	10 x 20
	0.79822(+1.0712%)	442	55.778	4 x 50
McCoy's Solution(7)	0.78796			

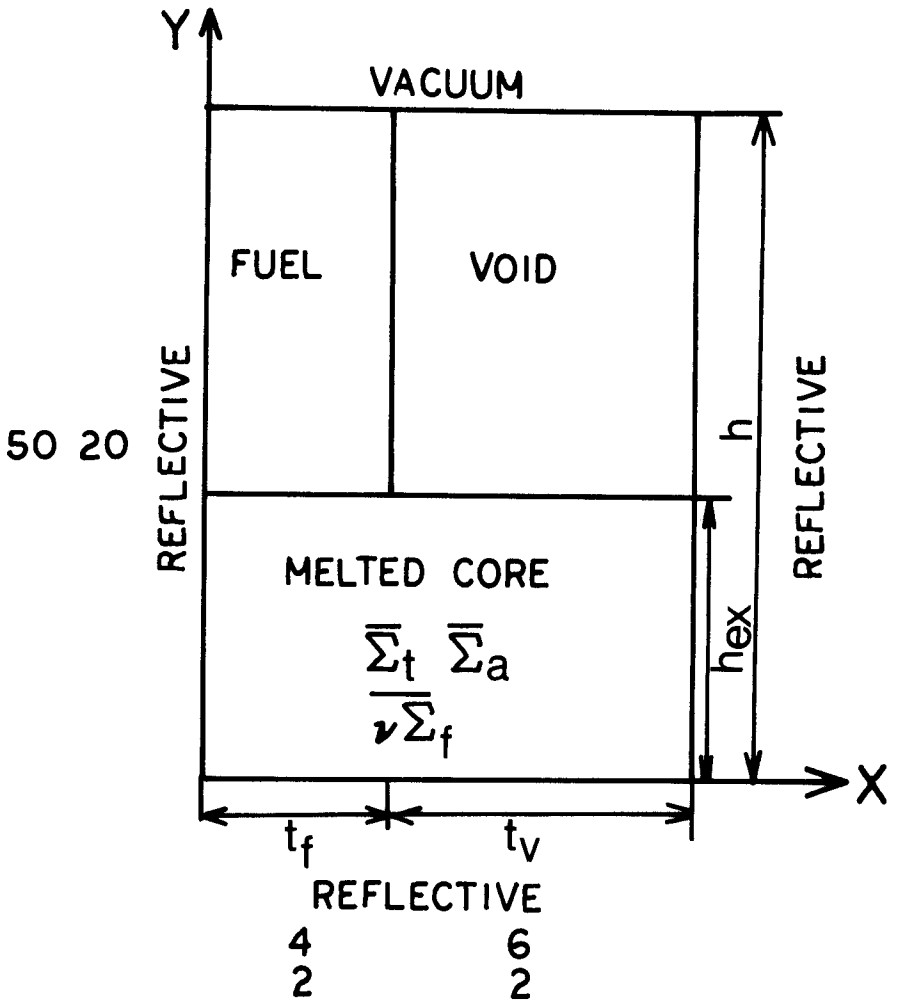

Fig. 11 Geometry and cross sections for Problem 6.

6. DISCUSSION AND CONCLUSIONS

First, we note that the spatial treatment of the discrete cones method is similar to the step characteristic scheme (SC) described in a paper by K.D. Lathrop.[11] The only difference between these two schemes is the treatment of the direction angle; the SC scheme employs the discrete ordinates approximation. Lathrop observed through numerical experiments that the SC scheme results in a larger leakage and a smaller absorption than those by the S_N method with the diamond difference scheme (DIAMF). Moreover, he observed that the total absorption by the SC scheme converges to the exact solution more slowly than that by the DIAMF scheme as the spatial mesh cells are refined. These observations agree with tendencies of solutions by the discrete cones method.

Although he did not do theoretical analyses on his observations, groups at Los Alamos and in India have investigated the convergence rate of proposed spatial difference schemes including the DIAMF and SC schemes since Lathrop's paper.[12-14] Their analyses are restricted to solutions in slab geometry; however, we may obtain rough pictures of numerical properties of the SC scheme in two dimensions from the results. They concluded that the DIAMF and SC schemes have second order accuracy for cell average and cell edge fluxes with respect to spatial discretization.

From this conclusion, along with Lathrop's, we conjecture that for spatial discretization the DC_N method in X-Y geometry has the same or somewhat lower order of accuracy than the DIAMF scheme. Furthermore, we see stronger effects of the order of the DC_N approximation on the accuracy for a given size of the spatial mesh cell. These must be thoroughly analyzed in the future.

Besides the ray effects, we must overcome a difficulty associated with deep penetration problems. In deep penetration problems a large number of

spatial mesh cells are required to obtain sufficiently accurate solutions because the mean free path is much shorter than the characteristic length of the system and schemes such as DIAMF, SC, and DC_N need a much smaller mesh cell than the mean free path to achieve accuracy. Consequently, the calculations become very costly. To overcome this difficulty, a computational scheme must have the property of faster convergence of iterations for a coarse mesh.

To accelerate the iteration, the diffusion synthetic method (DSA) was proposed[15] and implemented in some S_N codes. On the other hand, to provide the capability of a coarse mesh, Larsen and Alcouffe employed the linear characteristic scheme (LC) for X-Y geometry,[9] and it was found that their method is compatible with the DSA algorithm. Applying the DSA and LC schemes to the DC_N approximation, we will obtain the DC_N method with a higher order convergence rate for a coarse mesh than that of the current DC_N method. Such an extension will be carried out in the future.

Finally, we mention applications of the DC_N method to curved geometries. Such applications are necessary from a practical point of view, but it is very difficult to find elements of the transfer and escape matrices analytically. Even if they were obtained by numerical integration, the computing efficiency of the new method might be much worse than that of conventional methods as we see in applying the DC_N method of a void to R-Z geometry.

Acknowledgment

Support for this work has been provided by the United States Department of Energy.

References

1. Y. Watanabe and C.W. Maynard, "The Discrete Cones Method in Two-Dimensional Neutron Transport Computation," University of Wisconsin Fusion Technology Institute Report UWFDM-574, May 1984.

2. Y. Watanabe and C.W. Maynard, "The DC_N-S_N Hybrid Method for Two-Dimensional Neutron Transport Computation in R-Z Geometry," University of Wisconsin Fusion Technology Institute Report UWFDM-595, October 1984.

3. K.D. Lathrop and F.W. Brinkley, "TWOTRAN-II: An Interface, Exportable Version of the TWOTRAN Code for Two-Dimensional Transport," Los Alamos Scientific Laboratory Report LA-4848-MS (1973).

4. M. Abramowitz and I.A. Stegun, Handbook of Mathematical Functions, Dover Pub. Inc., New York (1972), p. 228, Eq. 5.1.1.

5. M. Abramowitz and I.A. Stegun, ibid., p. 231.

6. M. Abramowitz and I.A. Stegun, ibid., Eq. 25.4.30 on p. 887 and Table 25.4 on p. 916.

7. B.G. Carlson, "Tables of Equal Weight Quadrature EQ_N Over the Unit Sphere," Los Alamos Scientific Laboratory Report LA-4734 (1971).

8. Los Alamos Scientific Laboratory Group X-6, "MCNP - A General Monte Carlo Code for Neutron and Photon Transport," Los Alamos Scientific Laboratory Report LA-7396-M (1979).

9. R.E. Alcouffe and E.W. Larsen, "The Linear Characteristic Method for Spatially Discretizing the Discrete-Ordinates Equations in (X-Y) Geometry," Proc. Int. Topl. Mtg. Advances in Mathematical Methods for the Solution of Nuclear Engineering Problems, Munich, Germany, April 27-29, 1981.

10. E.M. Gelbard, "Streaming in Lattices," in Advances in Nuclear Sciences and Technology, Vol. 15, J. Lewins and M. Becker, eds., Plenum Press, New York (1983).

11. K.D. Lathrop, "Spatial Differencing of the Transport Equation: Positivity vs. Accuracy," J. Comp. Phys. 4, 475-498 (1969).

12. R.E. Alcouffe, E.W. Larsen, W.F. Miller and B.R. Wienke, "Computational Efficiency of Numerical Methods for the Multigroup, Discrete-Ordinates Neutron Transport Equations: The Slab Geometry Case," Nucl. Sci. Eng. 71, 111-127 (1979).

13. E.W. Larsen and W.F. Miller, "Convergence Rates of Spatial Difference Equations for the Discrete-Ordinates Neutron Transport Equations in Slab Geometry," Nucl. Sci. Eng. 73, 76-83 (1980).

14. S.M. Lee and R. Vaidyanathan, "Comparison of the Order of Approximation in Several Spatial Difference Scheme for the Discrete-Ordinates Transport Equation in One-Dimensional Plane Geometry," Nucl. Sci. Eng. 76, 1-9 (1980).

15. R.E. Alcouffe, "Diffusion Synthetic Acceleration Methods for the Diamond-Differenced Discrete-Ordinates Equations," Nucl. Sci. Eng. 64, 344-355 (1977).